Diffusive solvent dynamics in a polymer gel electrolyte studied by quasielastic neutron scattering

ARTICLE *in* THE JOURNAL OF CHEMICAL PHYSICS · JULY 2005

Impact Factor: 2.95 · DOI: 10.1063/1.1931568 · Source: PubMed

6 AUTHORS, INCLUDING:

Jan Swenson
Chalmers University of Technology
177 PUBLICATIONS **3,992** CITATIONS

SEE PROFILE

William Spencer Howells
Science and Technology Facilities Council
268 PUBLICATIONS **3,408** CITATIONS

SEE PROFILE

Lars Börjesson
Chalmers University of Technology
329 PUBLICATIONS **6,482** CITATIONS

SEE PROFILE

Diffusive solvent dynamics in a polymer gel electrolyte studied by quasielastic neutron scattering

D. Andersson,[a] D. Engberg, J. Swenson, and C. Svanberg
Department of Applied Physics, Chalmers University of Technology, SE-412 96 Göteborg, Sweden

W. S. Howells
Rutherford Appleton Laboratory, Chilton, Didcot OX11 0QX, United Kingdom

L. Börjesson
Department of Applied Physics, Chalmers University of Technology, SE-412 96 Göteborg, Sweden

(Received 3 March 2005; accepted 13 April 2005; published online 20 June 2005)

A quasielastic neutron scattering study has been performed on a polymer gel electrolyte consisting of lithium perchlorate dissolved in ethylene carbonate/propylene carbonate and stabilized with poly(methyl methacrylate). The dynamics of the solvent, which is crucial for the ion conduction in this system, was probed using the hydrogen/deuterium contrast variation method with nondeuterated solvent and a deuterated polymer matrix. Two relaxation processes of the solvent were studied in the 10–400 μeV range at different temperatures. From analysis of the momentum transfer dependence of the processes we conclude that the faster process ($\sim$100 μeV) is related to rotational diffusion of the solvent and the slower process ($\sim$10 μeV) to translational diffusion of the solvent. The translational diffusion is found to be similar to the diffusion in the corresponding liquid electrolyte at short distances, but geometrically constrained by the polymer matrix at distances beyond $\sim$5 Å. The study indicates that the hindered diffusion of the solvent on a length scale of the polymer network interchain distance ($\sim$5–20 Å) is sufficient to explain the reduced macroscopic diffusivity and ion conductivity of the gel electrolyte compared to the liquid electrolyte.
 [DOI: 10.1063/1.1931568]

I. INTRODUCTION

Electrochemical cells are increasingly being used for energy storage and as mobile sources of electricity. In applications where low weight and small size are important factors, lithium batteries are a common choice due to their high energy density. A typical electrolyte in these batteries is a salt dissolved in an organic solvent with high dielectric constant. It would, however, be preferable from safety, design, and mechanical perspectives to use solid electrolytes. The polymer electrolytes,[1] where the salt is dissolved in a polar polymer, e.g., a polyether, have several inherently attractive properties such as high mechanical and chemical stabilities, flexibility, and ease of manufacturing. The conductivity of a polymer electrolyte is closely linked to the polymer segmental mobility,[2] and therefore considerably lower than those of liquid electrolytes. Despite intensive research, it has not yet been possible to combine the inherent attractive properties of a pure polymer/salt electrolyte with a conductivity that is acceptable for room temperature applications.

This has spurred interest in another class of solid electrolytes, which are formed by immobilizing a liquid electrolyte in a polymer matrix. Several systems based on this approach have been developed with various polar nonaqueous organic liquid based electrolytes and, e.g., poly(vinylidene fluoride) (PVDF),[3,4] poly(acrylonitrile) (PAN),[5] or poly(methyl methacrylate) (PMMA) (Ref. 6) as the stabilizing polymer. One such polymer gel electrolyte based on PMMA and lithium perchlorate ($LiClO_4$) in propylene carbonate (PC) as electrolyte was first reported by Iijima *et al.*[7] This polymer gel electrolyte and a similar system with a mixed solvent of ethylene carbonate (EC) and PC has been studied in some detail using different techniques.[8–14] Their ionic conductivities were found to be much higher than those of pure polymer electrolytes and only moderately lower than those of the corresponding pure liquid electrolytes.[8,10] Studies of the influence of the salt and polymer concentrations on the conductivity and viscosity,[8,9] and spectroscopic studies[11,12] suggest a picture of these gel electrolytes as liquid electrolytes encaged in inert polymer matrices, when the polymer concentration is below 35%.

Another study was made on the polymer gel electrolyte using photon correlation spectroscopy (PCS) to probe the microscopic dynamics of the solvent and the polymer matrix. It was found that the gel has a complicated dynamical response[14] with a diffusive process that is proportional to the ion conductivity, while the segmental motion of the polymer is almost completely decoupled from the conductivity properties. The study thus supports a picture where the polymer gel electrolyte resembles a liquid electrolyte concerning the ion conduction mechanism, while the polymer matrix provides mechanical stability in line with the previous findings.[8,9,11,12] However, studies of the same gel electrolyte using NMR (Ref. 13) show that the immediate environments around the ions differ significantly between the gel and the liquid electrolytes, ruling out the presence of microscopic

[a]Electronic mail: dma@fy.chalmers.se

regions of pure liquid electrolyte in the gel electrolyte. The apparent contradictory results may reflect that the close environment of atoms is probed in NMR and the spectroscopic studies, while in PCS and the studies of transport properties, the dynamics is probed on a considerably longer length scale.

For the understanding of the conduction mechanism in polymer gel electrolytes it is, therefore, important to investigate the solvent dynamics on an intermediate length scale. An appropriate technique for this is quasielastic neutron scattering (QENS), which probes the dynamics in the picosecond range at molecular length scales. In the present paper we present results from the first study of a polymer gel electrolyte using QENS. The study focuses on the solvent dynamics in the gel and the paper is organized as follows: The next two sections, Secs. II and III, provide descriptions of the system and the experimental setup. In Sec. IV the dynamical processes that may be observed with QENS in the gel electrolyte are introduced. A model scattering function is presented that is used in the analysis of the neutron scattering data in Sec. V. Finally, the results are compared with those from other experimental techniques, and the implications for the understanding of the ion conduction mechanism are discussed.

II. THE GEL ELECTROLYTE

Polymer gel electrolytes are rather complex systems that have not previously been studied using QENS. The system we chose to study here, PMMA/EC/PC/$LiClO_4$, has the advantage that it has previously been investigated by various techniques.[8–23] In addition, spectroscopic studies have shown that this gel electrolyte is characterized by weak interactions between the solvent and the polymer matrix.[11,12] This is advantageous since too strong interactions may impede the ion conduction, and since a system with weak interactions is less complex and therefore suitable as a model system for a first study. When the specific polymer-solvent interactions are weak, we may concentrate on the effect on the solvent dynamics from the geometrical constraints of the polymer matrix.

The aim of the present study is to investigate the dynamics of the solvent within the gel, which is of relevance for the ion conduction. A method to selectively study one component of a sample in neutron scattering experiments is isotope substitution. Here, deuterated PMMA has been used, whereas the solvent was nondeuterated. The scattering is hence dominated by incoherent scattering from the protons of the solvent.

In the choice of solvent for a gel electrolyte chemical compatibility with the other cell materials is necessary. The stability *vis-à-vis* the lithium electrode requires that the solvent have no hydrogen donor groups (i.e., it must be aprotic). This excludes water which is otherwise a superb solvent for electrolytes. An ideal solvent should further have a high dielectric constant to promote ion dissociation, have a low viscosity to yield a high conductivity, and be nonvolatile. EC is a solvent that fulfills all these requirements. In the present system, EC is mixed with PC, which only differs from EC in having a methyl side group attached to the ethylene unit. In this way, crystallization, which takes place at 309 K in pure EC, is avoided. The advantage of mixed EC/PC over pure PC is that EC has a slightly higher dielectric constant than PC. Due to the chemical similarity between the molecules, the mixture can be expected to be close to ideal when there is no tendency for crystallization.

The electrolyte obtained by dissolving $LiClO_4$ in the EC/PC mixed solvent is highly dissociated. Molecular dynamics studies of this liquid electrolyte suggest that about four EC/PC molecules point their carbonyl oxygens towards each lithium ion in tetrahedral coordination.[24] For concentrations higher than one lithium ion per four solvent molecules, qualitative changes in the structure and behavior of the electrolyte were observed.[24,25] Recent *ab initio* calculations showed that the tetrahedral coordination of EC around the lithium ions is favored also in the gel electrolyte, and that lithium coordination to PMMA is much less frequent.[26]

Regarding the interaction between the liquid electrolyte and the polymer, experiments have generally shown that they are weak in PMMA- and PVDF-based gel electrolytes,[11,12,14,27] whereas PAN- and poly(ethylene oxide)-based electrolytes are characterized by stronger solvent-polymer interactions.[11,28,29] A detailed analysis of Fermi resonance perturbed Raman bands[15] did, however, show that the spectra of the gel electrolyte studied here demonstrate, in addition to solvent-solvent and solvent-cation couplings characteristic of liquid electrolytes, the presence of mixed states in which cations, solvent molecules, and polymer segments take part. The observed interaction appeared to be fairly strong, but of limited extent; the proportion of involved cations did not exceed 20%. Since no similar polymer-solvent interactions were observed in the corresponding salt-free system,[15] a possible interpretation is that the mixed states correspond to a small fraction of lithium ions which are not solely coordinated to solvent molecules, but also to a carbonyl oxygen of PMMA. Apart from the mixed states, the results of the study[15] support the view of weak polymer-solvent interactions also in the gel electrolyte.

III. EXPERIMENT

The polymer gel electrolyte was prepared by dissolving lithium perchlorate ($LiClO_4$) in a solution of EC and PC to form a liquid electrolyte. The liquid electrolyte was then immobilized into a polymer gel with high molecular weight PMMA. For the sample studied here deuterated PMMA (Polymer Source Inc., $M_W = 1\,587\,000$) has been used. The sample preparation follows standard gel preparation procedures described in Ref. 10. The initial materials used were of battery grade, i.e., of high purity and the water content was less than 50 ppm. The obtained sample was optically transparent and sealed under argon atmosphere. The average mole ratio of $LiClO_4$:EC:PC:PMMA in the sample was 4.5:46.5:19:30 where the PMMA ratio refers to the repeating unit. After complete gelation the sample was placed in a flat airtight aluminum cell with a sample thickness of 360 μm.

The thickness corresponds to 10% of the neutrons being scattered by the sample in its present orientation at 45° angle to the beam.

The measurements were performed on the IRIS time-of-flight backscattering spectrometer at the ISIS pulsed spallation source, Rutherford Appleton Laboratory, UK. The pyrolytic graphite 002 analyzer reflection used in the present study has a resolution (full width at half maximum) of 15 μeV and covers an energy window of ±0.4 meV and a Q range of 0.4–1.85 Å^{-1}. Measurements were performed at 253 K, 293 K, 333 K, and 373 K, which is well above the glass transition temperature of the liquid electrolyte ($T_g \approx 160$ K), but below T_g of bulk PMMA ($T_g \approx 380$ K). Due to the high atomic fraction of ^{1}H in the sample (0.25) and the large incoherent scattering cross section of ^{1}H, the incoherent scattering from the hydrogens of the solvent amounts to 81% of the total scattering. The scattering from PMMA amounts to only 10% of the total scattering due to the use of deuterated PMMA. Since the PMMA scattering is mainly coherent, this part is higher at peaks of the static structure factor of PMMA, e.g., around 1 Å^{-1}. Furthermore, the quasielastic scattering from PMMA in the present experimental window will be moderate as the glass transition temperature of bulk PMMA is high and the methyl group rotations do not give rise to any coherent scattering. The quasielastic scattering is thus predominantly incoherent scattering from the protons of the EC/PC solvent.

The 51 detectors were grouped into 10 or 16 groups, depending on the measurement time, to provide good statistics as well as coverage of the available Q window. Data corrections for absorption, background, and can scattering were performed using the on-site software package GUIDE.[30] Data from detectors in the plane of the sample ($Q \approx 1.7$ Å^{-1}), which suffer from severe self-shielding were discarded.

IV. MODEL OF THE MICROSCOPIC SOLVENT DYNAMICS OF GEL ELECTROLYTES

A preliminary analysis of QENS data from the polymer gel electrolyte was discussed in a previous paper.[31] The analysis included a fit of a scattering function consisting of an elastic peak and two Lorentzian peaks. The Q dependence of the widths and intensities of these peaks showed systematic trends suggesting a faster process with rotational character and a slower process with mainly translational character.

More detailed information on the individual dynamical processes requires an understanding of how they are reflected in the scattering. Here, it is highly likely that the solvent molecules exert both types of motion simultaneously. The corresponding scattering function $S(Q,\omega)$ is then not simply the sum, but instead the frequency convolution, of the scattering functions of the individual processes. To unravel the nontrivial relation between the Lorentzian peaks and the underlying dynamical processes that this infers, we construct a simple model based on the two processes of translational and rotational character, respectively, suggested from the preliminary analysis.[31] The aim is that the model should give a proper description of the essential behavior of the system and enable an analysis of the experimental data which considers both the linewidths and intensities in a consistent manner. In constructing the model scattering function, we begin by assuming that the statistical correlations between the translational, rotational, and vibrational motions of the solvent molecules can be neglected. This assumption is common in the analysis of QENS data since the intermediate scattering function for dynamically similar atoms is then simplified to a product of the component scattering functions:

$$\tilde{S}(Q,t) = S_{\mathrm{vib}}(Q,t)S_{\mathrm{rot}}(Q,t)S_{\mathrm{trans}}(Q,t). \tag{1}$$

Although the assumption is not perfectly valid here due to, e.g., dipole-dipole interactions in the solvent and correlated motions of solvent molecules in the coordination shell around the Li ions, it will suffice for the purposes of the present study where a simple model is needed. In our experimental window, $S_{\mathrm{vib}}(Q,t)$ essentially has the form of a Q-dependent constant, the well-known Debye–Waller factor. Since our focus is on the translational and rotational dynamics, we normalize by the Debye–Waller factor and get

$$S(Q,t) = \tilde{S}(Q,t)/S_{\mathrm{vib}}(Q,t) = S_{\mathrm{rot}}(Q,t)S_{\mathrm{trans}}(Q,t). \tag{2}$$

Next we must decide the general form to use for $S_{\mathrm{rot}}(Q,t)$ and $S_{\mathrm{trans}}(Q,t)$. In order to keep the model simple, we will follow a common route in the analysis of QENS data and use scattering functions for single relaxation time Debye processes, $S(Q,t)=A_0(Q)+[1-A_0(Q)]\exp[-t/\tau(Q)]$. The relaxation times of the processes are denoted $\tau_{\mathrm{rot}}(Q)$ and $\tau_{\mathrm{trans}}(Q)$, whereas $A_0(Q)=S(Q,t\rightarrow\infty)$, the elastic incoherent structure factors (EISF), are denoted $A_0^{\mathrm{rot}}(Q)$ and $A_0^{\mathrm{trans}}(Q)$, respectively. We note that free diffusion, like all dynamical processes where the particles can move without spatial restrictions, has a Q-independent intensity. The reason for not setting $A_0^{\mathrm{trans}}(Q)$ to 0 in spite of this is that the narrower Lorentzian peak, which was attributed to the translational process, demonstrated a decrease in intensity at low Q, which implies spatial confinement of the process and thus a Q-dependent intensity.

Now we consider how to combine the scattering functions of the rotational and translational processes in the overall scattering function. Here, the scattering is mainly incoherent and reflects the motion of the protons of the solvent. The relative fractions of protons which take part in the two processes are therefore relevant parameters for the model. The protons are considered in the model as either "static" or fully mobile, i.e., both translating and rotating; we have disregarded the possibility that protons participate in only one of the two processes to keep the model simple. The static protons may, e.g., represent molecules close to the matrix, which are essentially immobilized. The small amount of coherent elastic scattering from the matrix, which is not explicitly included in the model, will also be reflected in this term. The fraction of protons which are static is denoted x_s and the fraction of mobile protons x. ($x_s+x=1$.) The self-intermediate scattering function for the protons then has the following form:

$$S(Q,t) = x_s + xS_{\mathrm{rot}}(Q,t)S_{\mathrm{trans}}(Q,t)$$
$$= x_s + x\left\{A_0^{\mathrm{trans}}(Q) + [1 - A_0^{\mathrm{trans}}(Q)]\exp\left(\frac{-t}{\tau_{\mathrm{trans}}(Q)}\right)\right\}$$
$$\times\left\{A_0^{\mathrm{rot}}(Q) + [1 - A_0^{\mathrm{rot}}(Q)]\exp\left(\frac{-t}{\tau_{\mathrm{rot}}(Q)}\right)\right\}. \quad (3)$$

Next, we note from the preliminary analysis[31] that the rotational process is about a factor of 10 faster than the translational process. We therefore approximate the time dependence of the cross term in Eq. (3) by the time dependence of the pure rotational term and get a final simplified expression for the model scattering function with an elastic contribution and two quasielastic contributions of exponential character:

$$S(Q,t) = 1 - x[1 - A_0^{\mathrm{rot}}(Q)A_0^{\mathrm{trans}}(Q)]$$
$$+ xA_0^{\mathrm{rot}}(Q)[1 - A_0^{\mathrm{trans}}(Q)]\exp\left(\frac{-t}{\tau_{\mathrm{trans}}(Q)}\right)$$
$$+ x[1 - A_0^{\mathrm{rot}}(Q)]\exp\left(\frac{-t}{\tau_{\mathrm{rot}}(Q)}\right). \quad (4)$$

The corresponding model $S(Q,\omega)$ is then simply an elastic line and two Lorentzian peaks with Q-dependent widths, $1/\tau_{\mathrm{trans}}$ and $1/\tau_{\mathrm{rot}}$, and intensities as in Eq. (4).

In the following sections the modeling of the rotational and translational processes will be discussed in more detail. Based on relevant theoretical models for rotational and translational diffusions, we decide on the appropriate expressions to use for A_0^{trans} and A_0^{rot} in Eq. (4). Whereas the Lorentzian widths from the fit to the neutron scattering data correspond to $1/\tau_{\mathrm{rot}}$ and $1/\tau_{\mathrm{trans}}$ in Eq. (4), the correspondence to the characteristic times in the theoretical diffusion models is nontrivial since these models generally do not correspond to simple Debye processes. We examine the approximation involved in treating the processes as simple Debye processes in our model, and how the times τ_{rot} and τ_{trans} are related to the characteristic times in the theoretical diffusion models.

A. Uniaxial rotational diffusion

There are several theoretical models that describe rotational motion, e.g., jump rotation on a circle,[32,33] continuous rotational diffusion, and rotation on a sphere.[34,35] We will use the model for uniaxial rotational diffusion for the rotational process since it is a good description of the most likely origin of that process, the rotational motion of the solvent molecules with their strong dipole character. The differences between the various models for rotation are, however, limited and mainly occur at $Qr_{\mathrm{rot}} > 2$, where r_{rot} is the rotation radius. We have, for instance, also performed the analysis using the threefold jump rotation model that is often used in the analysis of QENS data, obtaining similar results.

The parameters in uniaxial rotational diffusion are the radius of rotation r_{rot} and the rotational diffusion constant D_{rot}, which has the dimension of inverse time. The corresponding isotropic self-scattering function is

$$S(Q,\omega) = A_0^{\mathrm{rot}}(Q)\delta(\omega) + \sum_{n=1}^{\infty} 2A_n^{\mathrm{rot}}(Q)\frac{1}{\pi}\frac{\tau_n}{1+\omega^2\tau_n^2}, \quad (5)$$

where

$$A_n^{\mathrm{rot}}(Q) = \frac{1}{2}\int_0^{\pi} J_n^2(Qr_{\mathrm{rot}}\sin\theta)\sin\theta\, d\theta \quad (6)$$

and

$$\frac{1}{\tau_n} = \frac{1}{\tau_1 n^2} = D_{\mathrm{rot}}n^2, \quad (7)$$

where the last identity shows the relation between τ_1 and D_{rot}, and J_n denotes the Bessel function of the first kind of nth order. A typical value of r_{rot} in the present case would be half the distance between opposite protons of an EC molecule, ~ 1.5 Å. The Q limit of the present experiment, ~ 2 Å^{-1}, thus corresponds to the region $Qr_{\mathrm{rot}} \lesssim 3$. In this region the main quasielastic contributions in the uniaxial rotational diffusion model are from $A_1^{\mathrm{rot}}(Q)$ and $A_2^{\mathrm{rot}}(Q)$.[32] The higher order terms increase in importance with increasing Q; the single Lorentzian representing rotation in our model [Eq. (4)] which best fits the composite scattering function, Eq. (5), over the experimental window will thus have a width $1/\tau_{\mathrm{rot}}$, which increases slightly with Q such that $1/\tau_1 \leqslant 1/\tau_{\mathrm{rot}}$. For a more detailed description of the uniaxial rotational diffusion model see, e.g., Ref. 32.

B. Restricted jump diffusion

We assume that the translational process corresponds to diffusive motion of the solvent. A microscopic description of diffusive processes is offered by jump diffusion models. Unbounded jump diffusion where the jump process is Poissonian with Gaussian distributed jump lengths, $\rho(\mathbf{r}) = \{1/[r_0\sqrt{(2\pi)^3}]\}\exp(-r^2/2r_0^2)$, has a single Lorentzian scattering function

$$S(Q,\omega) = \frac{1}{\pi}\frac{\Delta\omega(Q)}{[\Delta\omega(Q)]^2 + \omega^2}, \quad (8)$$

where

$$\Delta\omega(Q) = \frac{1}{\tau}\left[1 - \exp\left(-\frac{Q^2r_0^2}{2}\right)\right]. \quad (9)$$

The parameters are the characteristic jump length r_0 and the harmonic mean time between jumps, τ. The mean jump length is $\langle r^2\rangle = 3r_0^2$. Obviously, for the unbounded jump diffusion model $\tau_{\mathrm{trans}} = 1/\Delta\omega(Q)$ and $A_0^{\mathrm{trans}} = 0$.

We noted previously in this section that the intensity of the narrower peak decreases at low Q indicating that the translational process is somewhat hindered, which is plausible since the solvent moves in a matrix of PMMA. To consider the effect of hindered diffusion in the analysis, we use a model of random jump diffusion between parallel impermeable walls.[36] The motion perpendicular to the walls in this restricted jump diffusion model will display the qualitative features of diffusion bounded in three dimensions. The long-range diffusion which is obviously present in the system will be considered separately in the forthcoming analy-

sis. In addition to r_0 and τ, the system is now characterized by the distance between the walls of the bounded region L. The corresponding self-scattering function is

$$S(Q,\omega) = A_0^{\text{trans}}(Q)\delta(\omega) + \sum_{n=1}^{\infty} 2A_n^{\text{trans}}(Q)\frac{1}{\pi}\frac{\tau_n}{1+\omega^2\tau_n^2}, \quad (10)$$

where

$$A_n^{\text{trans}}(Q) = \frac{2(QL)^2[1-(-1)^n\cos(QL)]}{[(QL)^2-(n\pi)^2]^2} \quad (11)$$

and the widths are

$$\frac{1}{\tau_n} = \frac{1}{\tau}\left[1-\exp\left(-\frac{n^2\pi^2 r_0^2}{2L^2}\right)\right]. \quad (12)$$

The overall behavior in this model is at $Q > \pi/L$ similar to unbounded jump diffusion with, e.g., identical high Q asymptotic values for the width, $1/\tau$. At $Q < \pi/L$, the overall width does not tend to zero as for free diffusion, but instead approaches $1/\tau_1$. The single Lorentzian of Eq. (4) that best fits Eq. (10) thus has a width, $1/\tau_{\text{trans}}$, which increases with Q such that $1/\tau_1 < 1/\tau_{\text{trans}} < 1/\tau$.

In the present study, L is found to be ≈ 5 Å, i.e., within the experimental window, $QL < 10$. Then, the only significant quasielastic contributions in the restricted jump diffusion model are from $A_1^{\text{trans}}(Q)$, $A_2^{\text{trans}}(Q)$, and $A_3^{\text{trans}}(Q)$. In the present case, where r_0 and L are similar in size, the width will be significantly lower than $1/\tau$ only for the term with $n=1$ in Eq. (10). For a more detailed description of the model see, e.g., Ref. 36.

The use of a one-dimensional model to represent the hindered diffusion can be justified by comparison with an alternative model, continuous (i.e., not jump) diffusion in a sphere.[37] This model has, e.g., been used in a recent QENS study[38] of water diffusion in a perfluorosulfonated ionomer, a typical membrane material for fuel cells. Whereas the obvious jump character of the process at higher Q renders continuous spherical diffusion unfit to model the widths, the EISF $A_0^{\text{trans}}Q$ only reflects the geometry and should not differ between jump and continuous models. The two models have almost equal EISFs below the first minimum when $L = 1.5R$ where R is the radius of the confining sphere. At higher Q, the effect of representing the hindrance by a single characteristic length is more pronounced in the one-dimensional model with ripples in $A_0^{\text{trans}}Q$ which are attenuated by a factor ~ 10 in the spherical diffusion model. The difference, however, is not large and clearly outweighed by the advantage of the simultaneous consideration of jumps and spatial restriction in the restricted jump diffusion model.

V. RESULTS

The polymer gel electrolyte was measured at the temperatures 253 K, 293 K, 333 K, and 373 K. The total scattering intensity was found to be well described by a Debye–Waller expression, $I(Q) \propto \exp(-\langle u^2\rangle Q^2)$, where the root mean square displacement $\langle u^2\rangle^{1/2}$ is roughly proportional to the temperature and has a typical value of 0.55 ± 0.1 Å at 293 K.

Two Lorentzian peaks, an elastic line, and a background were fitted to the data using the QUASILINES program.[39] For details on the fitting procedure see Ref. 31. The fit and the quasielastic components are illustrated in Fig. 1. The parameters obtained from the fit are the widths and intensities of the Lorentzian peaks, and the intensity of the elastic line. The Q dependence of the widths [half width at half maximum (HWHM)] of the two Lorentzian peaks is shown in Fig. 2 for the temperatures 253 K, 293 K, 333 K, and 373 K. It is readily seen in the figure that the width of the broad peak, which is shown in the upper panel, has a weaker Q dependence than the width of the narrow peak shown in the lower

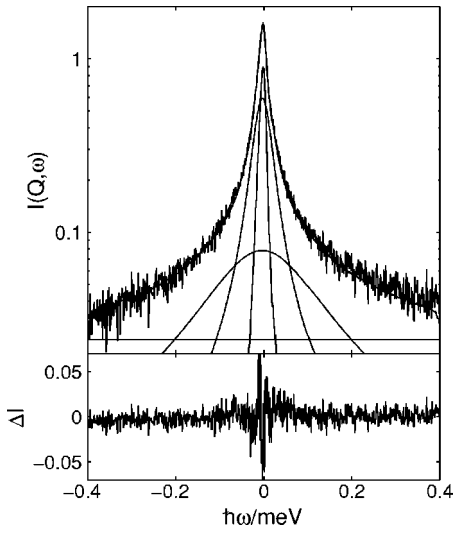

FIG. 1. The curve-fitting procedure is illustrated for $I(Q=1.27\ \text{Å}^{-1},\omega)$ at 293 K. The experimental data, the fit, and the components of the fit—two Lorentzian peaks, a static line, and background—are shown on a log scale. The fitted background was low, ~2%, and did not change significantly with temperature. Underneath the difference between data and fit is shown.

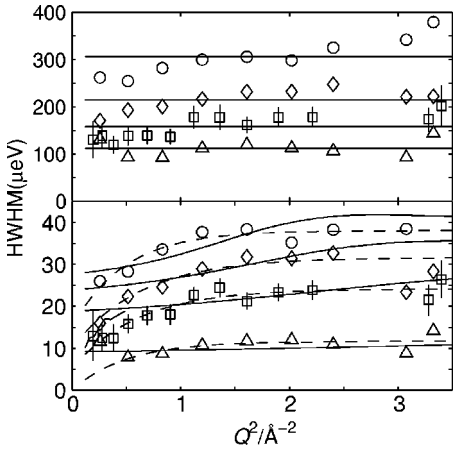

FIG. 2. Widths (HWHM) of the two quasielastic peaks; the upper panel corresponds to the faster rotational process while the lower panel corresponds to the slower translational process. Data corresponding to temperatures $T=253$ K (△), $T=293$ K (□), $T=333$ K (◇), and $T=373$ K (○) are shown in the graphs. For clarity, the points have been shifted by 5 and 50 μeV in the two panels, respectively. The widths (HWHM) of the peak of the translational processes are compared with a fit of the unbounded jump diffusion model with Gaussian jump length distribution, Eq. (9) (- - -), and with the widths from the restricted jump diffusion model, Eq. (10), with r_0 and L values according to Table I (—). For $T=293$ K, the effect on the predicted widths at low Q values of including 10% free diffusion in the hindered diffusion model is also shown.

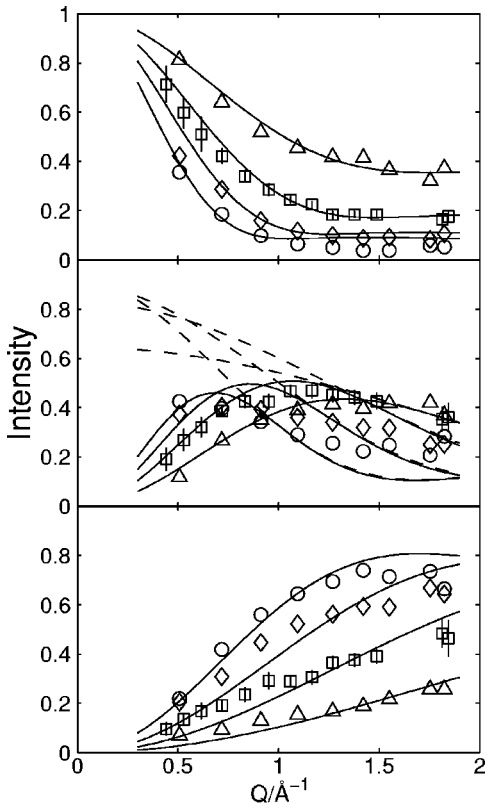

FIG. 3. Q dependence of the intensities of the quasielastic Lorentzian peaks and the elastic line normalized to the total integrated scattering intensity at 253 K (△), 293 K (□), 333 K (◇), and 373 K (○). The uppermost panel shows the elastic line, the lowermost one corresponds to the faster process, and the middle panel depicts the slower process. A fit to the relative peak intensities of the model, Eq. (4), with restricted jump diffusion, Eq. (11), and uniaxial rotational diffusion, Eq. (6) (—), is included. In the middle panel, we also show the intensities corresponding to free diffusion (- - -).

panel. The intensities of the elastic line and the two Lorentzian peaks are shown in Fig. 3. No significant contribution of coherent scattering from the polymer is discernible in the intensity of the elastic line.

Based on the quality of the fits, the separation in widths, and the regular trends of the obtained parameters, the two quasielastic peaks from the fit are assumed to correspond to two distinct dynamical processes. The faster process is, from the almost Q-independent width and the increasing intensity with Q, identified as rotation, presumably of the solvent molecules. The slower process is identified as some kind of translational diffusion from the increasing width with Q at low Q. We also see that the intensity of the narrow peak decreases at low values of Q, indicating that the translational diffusion is spatially restricted, e.g., as a result of the geometrical constraints imposed by the PMMA matrix. It might be argued that this decrease is caused by the peak becoming narrower and finally not resolved by the instrument, but instead detected as elastic scattering. However, the resolution of IRIS (15 μeV) can easily resolve the peak widths we measure here. Thus, the observed decrease in intensity at low Q values is not just a resolution effect.

The correspondence between the fitted peaks and the underlying dynamical processes is, however, not direct; the intensity of the slower translational process is affected by the Q-dependent intensity of the faster rotational process. Our model from the preceding section implies that the characteristic times of the processes equal the inverse widths of the peaks, whereas the situation for the intensities of the peaks is more complicated, with a detailed relation between them and the elastic incoherent structure factors of the processes according to Eq. (4).

To obtain more information about the fundamental properties of the system that are reflected in the observed intensities, the model based on Eq. (4), with $A_0^{\mathrm{rot}}(Q)$ given by Eq. (6), and where $A_0^{\mathrm{trans}}(Q)$ is given by Eq. (11) was fitted to the intensities. The parameters used in the model are the rotation radius r_{rot}, the confinement length L, the characteristic jump length r_0, the fraction of mobile protons x, and the characteristic times of the two processes, τ_{trans} and τ_{rot}. The parameters that affect the intensities are L, r_{rot}, and x, while L, r_0, and the characteristic times affect the widths. The intensities according to Eq. (4) are fitted simultaneously to the experimental intensities of the two quasielastic peaks and the elastic line, giving values for L, r_{rot}, and x at the different temperatures. We now consider the two processes separately, starting with the rotational process.

The rotational process dominates the short-time behavior. From Fig. 2 we deduce nearly Q-independent characteristic times, shown in the figure as lines corresponding to $\tau_{\mathrm{rot}}\,(\mathrm{ps}) = 5.9$, 6.1, 5.7, and 4.2 in order of increasing temperature. The Q dependence of the intensity of the broad peak corresponding to rotation, along with the fit of the model [Eqs. (4), (6), and (11)], are shown in the bottom part of Fig. 3. Clearly, the maximum of the intensity shifts towards lower Q values with increasing temperature. The corresponding radii of rotation from the fit are, in order of increasing temperature, $r_{\mathrm{rot}}\,(\mathrm{Å}) = 0.7$, 1.0, 1.3, and 1.7, respectively. The uncertainty of the values are rather large, particularly for the lowest temperature. Were it the same entity rotating at all temperatures, one would expect r_{rot} to be constant. A likely explanation why r_{rot} increases with temperature and why only a very weak temperature dependence is observed for τ_{rot} is that the system is complicated with different molecules in different local environments, which obviously means that r_{rot} corresponds to some weighted average radius of rotation of the rotating entities that are visible in the experimental window at a specific temperature. The observed change of r_{rot} with temperature may also reflect other degrees of freedom that are not explicitly included in the model.

We now turn to the process of main interest: the slower process that has been identified as hindered translational diffusion, due to the decrease in the intensity of the corresponding Lorentzian peak at low Q. The parameters related to this process in the model [Eqs. (4) and (11)] are L and the jump diffusion parameters r_0 and τ. The confinement length was obtained from the fit of the model to the intensities as shown by solid lines in Fig. 3. The values of L are shown in Table I and are typically around 5 Å.

The other parameters, r_0 and τ, only affect the width. However, since the width in the restricted jump diffusion model, Eq. (10), depends on both r_0 and L, it is difficult to obtain reliable values for r_0 from a fit of this model to the

TABLE I. Fitted parameters are the fraction of mobile protons x, the (harmonic) mean residence time for translational diffusion τ, the translational diffusion coefficient D_{trans}, and the confinement length L.

T (K)	x	τ (ps)	D_{trans} (m^2/s)	L (Å)
253	0.65	56	3.6×10^{-10}	3.60
293	0.83	34	4.8×10^{-10}	4.25
333	0.90	30	5.1×10^{-10}	5.01
373	0.92	29	6.9×10^{-10}	5.97

widths over the rather limited experimental Q window. Instead, we note that r_0 and τ are local properties which should only be weakly influenced by the confinement as has, e.g., been observed in a QENS study of water in poly(vinyl alcohol).[40] The widths for the restricted and unbounded jump diffusion models are also similar for $Q>2\pi/L$. An alternative strategy is therefore to determine r_0 and τ using the unbounded jump diffusion model, Eq. (9), and then check the consistency of the obtained parameters with the restricted jump diffusion model. We then see that the width of the narrow peak can be rather well described by the unbounded jump diffusion model, as shown by dashed lines in the lower panel of Fig. 2.

The parameters obtained from the fit of the unbounded jump diffusion model are the harmonic mean residence time τ and the rms jump length $\langle r^2\rangle^{1/2}=\sqrt{3}r_0$. The rms jump length is $\approx$2 Å and shows no significant dependence on temperature. A similar observation of a temperature independent jump distance has been made in a QENS study of water.[41] We therefore expect τ to be more important for the temperature dependence of the diffusivity. The values of τ are shown in Table I, together with values for the corresponding translational diffusion constant $D_{\text{trans}}=\langle r^2\rangle/(6\tau)$.

We now check the consistency of r_0 with the restricted jump diffusion model. The width corresponding to the restricted jump diffusion model can be determined by fitting a Lorentzian function to the scattering function, Eq. (10), over the experimental ω window. This was done using the obtained values for L and r_0, whereas τ, which does not affect the Q dependence of the width but only the magnitude, was kept free. The obtained widths are shown in Fig. 2, lower panel as solid lines. The shown widths correspond to a ratio between τ for restricted diffusion and τ for unbounded diffusion of 1.2 for the three highest temperatures and 1 for the lowest one.

The restricted jump diffusion model thus provides a slightly worse description of the widths than does the unbounded jump diffusion model. Note, however, that the intensity of the narrow peak does not agree at all with free diffusion, as can be seen in the middle panel of Fig. 3 where the intensities according to unbounded jump diffusion [$A_0^{\text{trans}}(Q)=0$ in Eq. (4)] are included as dashed lines. A likely reason why the width of the narrow peak resembles that for unbounded diffusion also at low Q values is that some free diffusion occurs in the system which will have a large effect on the observed widths. The effect on the width of the narrow peak, determined as above, when a small component of unbounded diffusion, Eq. (8), is added to the restricted diffusion, Eq. (10), is shown in Fig. 2 for $T=293$ K at low Q.

We have thus demonstrated that the restricted jump diffusion model can consistently describe the behavior of the intensity, whereas unbounded diffusion fails. Still, the Q dependence of the width of the narrow peak shows that the translational diffusion is not fully confined. Overall, this shows that the slower process mainly corresponds to hindered diffusion [Eqs. (10) and (11)], but with some component of free diffusion [Eqs. (8) and (9)].

VI. DISCUSSION

The analysis of QENS data of a complex system like the present, where no prior models exist, is a daunting task. The nature of the system, with a mixed solvent with dissolved salt in the intricate topology of the polymer matrix, is likely to impose a degree of heterogeneity to the dynamical processes of the solvent. Our response has been to analyze the data, which could be described in terms of an elastic line and two quasielastic peaks, within a simplified model that contains the main dynamical processes we expect from a preliminary analysis to be relevant for the observed dynamics of the solvent, namely, rotational and hindered translational diffusive motions. To test the model, we consider simultaneously the Q-dependent intensities and widths of the peaks. Through the analysis we are able to determine three characteristic lengths r_{rot}, r_0, and L and two characteristic times τ_{trans} and τ_{rot} that describe the microscopic dynamics of the solvent in the picosecond-nanosecond range.

The rotational process is characterized by a rotational radius which increases with temperature and a characteristic time with a weak temperature dependence. The choice of the uniaxial rotational diffusion model to describe the process was based on the assumption that the process mainly corresponds to rotational diffusion of the solvent molecules, but other rotational processes are conceivable: EC and PC exhibit a ring inversion with an energy barrier of $\sim$50 meV (Ref. 42) and a proton displacement corresponding to $r_{\text{rot}}\sim0.3$ Å; the methyl groups of the PC molecules may also rotate and then contribute at $r_{\text{rot}}\sim1$ Å. Although the statistics of the data and the Q range of the current experiment practically prohibit the extraction of more information than the single effective r_{rot} value, these processes can be dismissed as the main origin of the rotational process; the ring inversion will, due to the small proton displacement, appear effectively static (EISF$\approx$1) in the present experimental window, and only 19% of the protons are located in the methyl groups of PC. We will later provide a comparison of the time scales for the rotational and translational processes, which further support that rotational diffusion of the solvent molecules plays the dominant role in the rotational process.

We now consider the translational diffusion process. An alternative representation of the intensity data for this process, where the influence from the Q dependence from the faster rotational process is removed, is obtained when the intensity of the narrow peak, shown in the middle panel of Fig. 3, is divided by xA_0^{rot}. In this representation the intensity for free diffusion should be Q independent according to Eq.

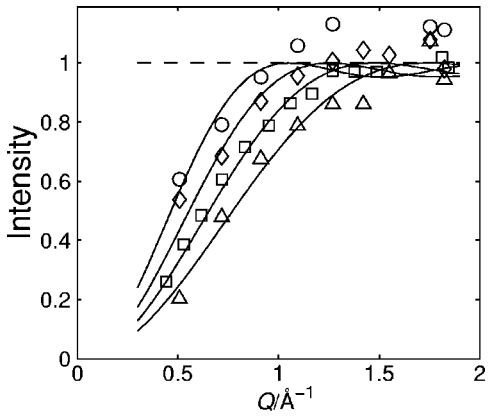

FIG. 4. The data for the narrow peak has been divided by the fitted values of $xA_0^{\mathrm{rot}}(Q)$ to display the intensity corresponding to the translational diffusion process undistorted by the rotation. Full lines are fits of $1-A_0^{\mathrm{trans}}(Q)$ of the restricted diffusion model, Eq. (10), to the normalized intensity, while the dashed line is the intensity corresponding to unbounded diffusion, Eq. (8).

(4). These normalized intensities are shown in Fig. 4. Again, it is obvious that the restricted jump diffusion model provides a much better description of the intensity data than does the unbounded diffusion model. At high Q the data are smoother than the restricted jump diffusion model. The ripples in the model are the effect of representing the spatial hindrance by a single L value, whereas the real system is more heterogeneous. The effect is more pronounced in the one-dimensional model used here, see end of Sec. IV.

The temperature dependence of the diffusivity from Table I is shown in Fig. 5. The diffusivity of the polymer gel electrolyte studied here has previously been determined in experiments using PCS,[14] results which are also included in Fig. 5. The process observed in PCS has an exponential relaxation behavior and was identified as diffusion from its Q dependence. It can be seen that the diffusivity observed using PCS is considerably lower than the diffusivities found by QENS, but the gap between the diffusivities is narrowing at

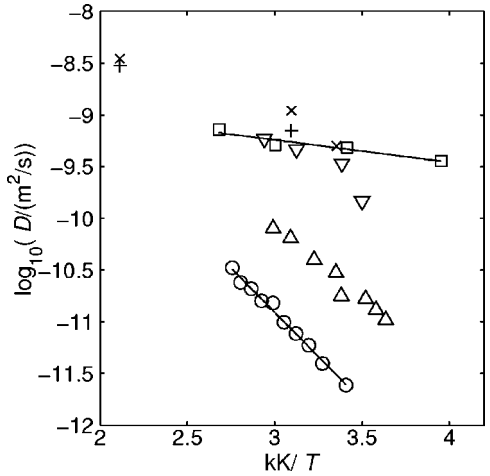

FIG. 5. The temperature dependence of the diffusive process in Arrhenius representation. Diffusivity from QENS (□) and PCS (○).[14] Nernst–Einstein diffusivities from impedance spectroscopy of the gel electrolyte (△) and liquid electrolyte (▽) (Ref. 44). MD values for EC (+) and PC (×) (Ref. 45).

the highest temperatures.[43] It is, however, difficult to compare the two, since the techniques differ largely in the length scales they probe (PCS ~ 1 μm, QENS ~ 5 Å), and PCS measures a collective diffusion within the gel whereas the self-diffusion of the solvent is measured in the present incoherent quasielastic neutron scattering study. In Fig. 5 we have also included conductivity σ results from dielectric measurements of the present gel electrolyte and the corresponding liquid electrolyte[44] in the form of the diffusivity obtained using the Nernst–Einstein equation, $D_\sigma = \sigma k_B T / N q_e^2$.

The long-range collective diffusivity observed using PCS is nearly proportional to the conductivity from the dielectric measurement of the gel electrolyte, whereas the higher short-range diffusivity observed using QENS is in a close agreement with the dielectric conductivity results for the liquid electrolyte. The QENS diffusivity of the gel electrolyte may also be compared with diffusion data[45] calculated by molecular dynamics (MD) for pure EC and PC (marked in Fig. 5); the difference is limited compared with the much larger difference for the long-range diffusion.

Considering that the ion conduction takes places in the solvent, the similar temperature dependence of the conductivity and the collective diffusion probed by PCS indicate that they are both proportional to the solvent diffusion. It has been proposed that the temperature dependence of the solvent and collective diffusion in a polymer gel can both be described by Stokes–Einstein relations, Eq. (13), but with different characteristic length scales: the hydrodynamic radius of the solvent molecules, r_s, for the solvent diffusion, and the dynamical screening length for the hydrodynamic interactions, ξ_h, for the collective diffusion.[46] The effect of the polymer network on the long-range diffusion is then, in Eq. (13), represented by an effective viscosity that is higher than the bulk solvent viscosity. Typically, ξ_h is 20–30 Å in a PMMA gel at the present concentration,[47] whereas the hydrodynamic radius of the solvent molecule is 1–2 Å. The expected ratio between the solvent diffusivity and the collective diffusivity is then $\xi_h / r_s \approx 20$. Concerning the solvent diffusion and the ion conductivity, an idea of the relation between the two can be obtained from a pulsed field gradient NMR study of the polymer gel electrolyte PVDF/N,N-dimethyl formamide/$LiCF_3SO_3$, where the diffusivities of the solvent, cations, and anions were measured separately.[27] At a polymer:solvent:salt ratio similar to that of the presently investigated gel electrolyte, the ion diffusivities were found to be approximately half that of the solvent. Overall, this suggests that D_σ should be ca. ten times larger than the collective diffusivity probed by PCS, which is in a good agreement with the data in Fig. 5.

The similarity between the diffusivity within the confined regions (~ 5 Å) in the gel electrolyte as determined in the present QENS study and the diffusivities of the liquid electrolyte and of pure EC/PC indicates that, on this short length scale, the dynamics of the solvent resembles the dynamics of the liquid electrolyte and the effects from interactions with the polymer are rather limited, in line with the spectroscopic studies where no strong interactions between PMMA and the solvent were observed.[11,12] Similar

local dynamics is also supported by dielectric data of the relaxation time of the α process in pure PC and PC with 30% PMMA (a system analogous to the gel electrolyte of the present study, but with no salt).[48] The study showed ~10 times slower dynamics in the gel at lower temperatures, 165 K–180 K, but an extrapolation of the observed temperature dependence to the presently investigated temperatures predicts a much smaller difference between the relaxation times (less than a factor of 2), in agreement with our conclusion.

The static scattering which persists to the highest Q values of the experimental window of the present QENS study, and which we interpret as a fraction of less mobile solvent molecules, is, however, in difference to the expected behavior of the liquid electrolyte. The fraction of less mobile solvent molecules, according to our analysis, ranges from 8% at 373 K to 35% at 253 K. A spectroscopic study of Fermi resonance perturbed Raman bands[15] of a gel electrolyte with the same composition as the presently investigated one but with lithium bis(trifluoromethane sulfone imide) in place of $LiClO_4$, showed the presence of mixed states in which cations, solvent molecules, and polymer segments take part, whereas no mixed states involving the polymer and the solvent were found in the corresponding salt-free system. The proportion of cations involved in the mixed states found in that study did, however, not exceed 20%, which with a fourfold coordination of EC/PC to Li^+ corresponds to less than 6% of the solvent molecules in the gel electrolyte. The presence of polymer/solvent complexes has also been shown in syndiotactic PMMA gels (without salt) by a combination of differential scanning calorimetry, neutron diffraction, and NMR.[49,50] The complexes were interpreted as solvent molecules trapped within polymer helices formed under gelation, and the complexes typically consisted of two solvent molecules per three PMMA monomers. It is difficult to tell how the static scattering observed in the present QENS study is related to the mixed states observed in the spectroscopic study[15] or the presence of similar complexes to those observed in the *s*-PMMA gel.[49,50] The fraction of less mobile solvent (8%–35%) determined from the QENS data using the model is rather high to be explained solely by the complexes involved in the mixed states from the spectroscopic study. The fraction is more consistent with the complexes observed in *s*-PMMA gels; in our case similar complexes with two solvent molecules per three PMMA monomers, would correspond to 29% complexed solvent, if all PMAA were complexed.

Next we consider the length scale of the constrained diffusion. The values of the confinement length L (Table I) agree well with an expected length scale for the solvent confinement in the gel: small angle neutron scattering (SANS) data[51] show a typical length scale of 10 Å at 293 K for the center-to-center distance for the polymer chains in the PMMA matrix of the present system, whereas the characteristic interchain distance in the absence of solvent is about 6 Å based on the position of the first diffraction peak at $Q \sim 1$ Å^{-1} in PMMA;[52] the 4 Å increase in the distance can be regarded as a static length scale characteristic of the space available for the solvent between the polymer chains.

The structural heterogeneity due to the polymer matrix should typically disappear beyond a couple of interchain distances, i.e, ~20 Å. Is this heterogeneity at ~5–20 Å enough to explain the difference between the short-range diffusion, as observed by QENS, and the long-range diffusion that determines the ion conduction? The difference is about a factor of 10. The quantitative effect of the structural heterogeneity on the diffusion corresponds, within the simplified picture of this study, to the relative amounts of hindered and free diffusion. Whereas the intensities could in the present analysis be interpreted assuming only hindered diffusion, the widths clearly indicated the presence of free diffusion. The effect of even a small amount of free diffusion on the observed widths is, however, large within the limited experimental window of the present study. We therefore refrain from giving a precise estimate of the ratio of free diffusion, but due to the successful analysis of the intensities, we consider it unlikely that the ratio significantly exceeds 0.1. The heterogeneity due to the polymer matrix is then sufficient to explain the difference between the microscopic and the macroscopic diffusivities; no other suggested length scales of heterogeneity need to be invoked. For instance, SANS results[51] have indicated structural heterogeneity in the polymer gel electrolyte at a length scale of ~200 Å, and an upper length scale for dynamical heterogeneity was suggested by recent PCS studies[53] in which a crossover to anomalous diffusion within the salt-free polymer gel was observed above a certain Q value corresponding to a length scale of typically a few thousand angstroms. Our interpretation suggests that, while these length scales may be of great importance for the structure and collective diffusion (probed by PCS) respectively, they are of limited importance for the self-diffusion of the solvent.

Finally, we investigate the relation between the two processes to see whether the attribution of them to translational and rotational diffusion of the solvent is plausible. In molecular liquids well above the glass transition, rotational and translational diffusive motion are related in a way usually rather well described by the Stokes–Einstein and Debye–Stokes–Einstein equations. These equations, which are derived from fluid mechanics, involve the local viscosity η and the Stokes radius r_s describing the effective hydrodynamic size of the molecules. Despite their macroscopic derivation, they are usually correct within an order of magnitude:

$$D_{\mathrm{trans}} = \frac{k_B T}{6\pi\eta r_s}, \quad \tau_{\mathrm{rot}} = \frac{4\pi\eta r_s^3}{3k_B T}. \tag{13}$$

The product of the rotational correlation time and the translational diffusivity should thus be a constant of the order of the Stokes radius squared:

$$D_{\mathrm{trans}}\tau_{\mathrm{rot}} = \tfrac{2}{9} r_s^2. \tag{14}$$

According to Eq. (13), D_{trans} and $1/\tau_{\mathrm{rot}}$ should also have the same temperature dependence and be proportional to T/η. If the two processes are assumed to correspond to translation and rotational diffusion of the solvent molecules, and using the values for D_{trans} and τ_{rot} from our previous analysis in Eq. (14), we obtain $r_s \approx 1.1$ Å, i.e., only a slight underestimate of the size of the solvent molecules; the attribution thus seems reasonable.

VII. CONCLUSIONS

In this first QENS study of a polymer gel electrolyte, we utilize the strength of neutron scattering to simultaneously provide information on both the spatial and temporal behaviors of the system. We identify two dynamical processes in the picosecond-nanosecond range: a faster one of rotational character and a slower one of translational character. A drop in intensity at low Q of the peak corresponding to the translational process indicated that the process is spatially constrained. It was also shown that a model for free diffusion is unable to describe the Q dependence of the intensities for the investigated polymer gel electrolyte.

Based on the identification of the processes, a simplified model was instead devised where the rotational process was modeled as uniaxial rotational diffusion and the translational process as spatially restricted jump diffusion. The model provides a consistent description of the observed intensities of the processes, whereas the description of the linewidths is not improved compared with a model based on free diffusion.

The obtained results are consistent with the translational and rotational processes being the diffusive motion of the solvent molecules. The observed diffusive dynamics has a time scale very similar to that of the pure liquid solvent. The effect of the polymer matrix is, however, seen at low Q corresponding to distances exceeding 5 Å, where long-range diffusion is impeded in the gel electrolyte. There is also a fraction of less mobile solvent molecules trapped in the gel. The results indicate that the heterogeneity on the length scale $\sim 5-20$ Å due to the polymer matrix is sufficient to explain the difference between the macroscopic diffusivity that determines the ion conductivity and the short-range, liquidlike, diffusivity observed by QENS, as well as the lower conductivity of the gel electrolyte compared to the corresponding pure liquid electrolyte. Only the lower end of the suggested region of heterogeneous solvent dynamics (~ 5 Å) was actually probed in the present study; the conclusions beyond this length scale are indicative only. To follow the diffusive process further into this region requires experiments which extend to lower Q values and have higher energy resolution than the present one.

ACKNOWLEDGMENTS

Financial support from the Swedish Natural Science Research Council and the Swedish Foundation for Strategic Research is gratefully acknowledged.

[1] F. M. Gray, *Polymer Electrolytes* (Royal Society of Chemistry, Cambridge, 1997).
[2] L. M. Torell and C. A. Angell, Br. Polym. J. **20**, 173 (1988).
[3] E. Tsushida, H. Ohno, and K. Tsunemi, Electrochim. Acta **28**, 591 (1983).
[4] K. Tsunemi, H. Ohno, and E. Tsushida, Electrochim. Acta **28**, 833 (1983).
[5] M. Watanabe, M. Kanba, K. Nagaoka, and I. Shinohara, J. Polym. Sci., Polym. Phys. Ed. **21**, 939 (1983).
[6] W. Wixwat, J. R. Stevens, A. M. Anderson, and C. G. Granqvist, *Second International Symposium on Polymer Electrolytes*, edited by B. Scrosati (Elsevier, Amsterdam, 1990), p. 461.
[7] T. Iijima, Y. Toyoguchi, and N. Eda, Denki Kagaku **53**, 619 (1985).
[8] O. Bohnke, G. Frand, M. Rezrazi, C. Rousselot, and C. Truche, Solid State Ionics **66**, 97 (1993).
[9] O. Bohnke, G. Frand, M. Rezrazi, C. Rousselot, and C. Truche, Solid State Ionics **66**, 105 (1993).
[10] G. B. Appetecchi, F. Croce, and B. Scrosati, Electrochim. Acta **40**, 991 (1995).
[11] D. Ostrovskii, A. Brodin, L. M. Torell, G. B. Appetecchi, and B. Scrosati, J. Chem. Phys. **109**, 7618 (1998).
[12] E. Cazzanelli, G. Mariotto, G. B. Appetecchi, F. Croce, and B. Scrosati, Electrochim. Acta **40**, 2379 (1995).
[13] P. E. Stallworth, S. G. Greenbaum, F. Croce, S. Slane, and M. Salomon, Electrochim. Acta **40**, 2137 (1995).
[14] C. Svanberg, G. B. Appetecchi, J. Adebahr, H. Ericsson, L. M. Torell, L. Börjesson, and B. Scrosati, J. Chem. Phys. **111**, 11216 (1999).
[15] D. Ostrovskii, M. Edvardsson, and P. Jacobsson, J. Raman Spectrosc. **34**, 40 (2003).
[16] O. Bohnke, C. Rousselot, P. A. Gillet, and C. Truche, J. Electrochem. Soc. **139**, 1862 (1992).
[17] Y. K. Yarovoy, H. P. Wang, and S. L. Wunder, Solid State Ionics **118**, 301 (1999).
[18] C. Svanberg, J. Adebahr, R. Bergman, L. Börjesson, B. Scrosati, and P. Jacobsson, Solid State Ionics **136**, 1147 (2000).
[19] C. Svanberg, R. Bergman, L. Börjesson, and P. Jacobsson, Electrochim. Acta **46**, 1447 (2001).
[20] M. Y. Qureshi, D. Berstan, G. G. Cameron, M. D. Ingram, and C. Rousselot, Polym. Int. **47**, 16 (1998).
[21] X. Liu and T. Osaka, Electrochemistry (Tokyo, Jpn.) **69**, 422 (2001).
[22] A. M. Christie and C. A. Vincent, J. Appl. Electrochem. **26**, 255 (1996).
[23] C. S. Kim and S. M. Oh, Electrochim. Acta **46**, 1323 (2001).
[24] J.-C. Soetens, C. Millot, and B. Maigret, J. Phys. Chem. A **102**, 1055 (1998).
[25] E. Cazzanelli, F. Croce, G. B. Appetecchi, F. Benevelli, and P. Mustarelli, J. Chem. Phys. **107**, 5740 (1997).
[26] P. Johansson, M. Edvardsson, J. Adebahr, and P. Jacobsson, J. Phys. Chem. B **107**, 12622 (2003).
[27] I. M. Ward, M. J. Williamson, H. V. St. A. Hubbard, J. P. Southall, and G. R. Davies, J. Power Sources **81**, 700 (1999).
[28] G. Fleischer, H. Scheller, J. Kärger, A. Reiche, and B. Sandner, J. Non-Cryst. Solids **235**, 742 (1998).
[29] J. Adebahr, P. Gavelin, P. Jannasch, D. Ostrovskii, and P. Jacobsson, Solid State Ionics **135**, 149 (2000).
[30] M. T. F. Telling and W. S. Howells, GUIDE–IRIS data analysis, RAL Technical Report No. RAL-TR-2000-004, (CCLRC Rutherford Appleton Laboratory, Didcot,2000).
[31] D. Andersson, C. Svanberg, J. Swenson, W. S. Howells, and L. Börjesson, Physica B **301**, 44 (2001).
[32] M. Bée, *Quasielastic Neutron Scattering: Principles and Applications in Solid State Chemistry, Biology and Materials Science* (Adam Hilger, Bristol, 1988).
[33] A. J. Dianoux, F. Volino, and H. Hervet, Mol. Phys. **30**, 1181 (1975).
[34] V. F. Sears, Can. J. Phys. **44**, 1279 (1966).
[35] V. F. Sears, Can. J. Phys. **45**, 237 (1967).
[36] P. L. Hall and D. K. Ross, Mol. Phys. **42**, 673 (1981).
[37] F. Volino and A. J. Dianoux, Mol. Phys. **41**, 271 (1980).
[38] A. M. Pivovar and B. S. Pivovar, J. Phys. Chem. B **109**, 785 (2005).
[39] W. S. Howells, IDA—Iris data analysis, RAL Technical Report No. RAL-TR-96-006, (CCLRC Rutherford Appleton, Didcot, 1996 (unpublished).
[40] G. Paradossi, F. Cavalieri, E. Chiessi, and M. T. F. Telling, J. Phys. Chem. B **107**, 8363 (2003).
[41] F. Cavatorta, A. Deriu, D. Di Cola, and H. D. Middendorf, J. Phys.: Condens. Matter **6**, A113 (1994).
[42] M. Masia, M. Probst, and R. Rey, J. Phys. Chem. B **108**, 2016 (2004).
[43] The lower temperature dependence for the short-range diffusivity obtained using QENS than for the long-range diffusivity in the gel electrolyte may reflect that the reduction in long-range solvent diffusion due to the polymer matrix is more pronounced at lower temperatures. However, the temperature dependence is low also in comparison with bulk liquids, which indicates that it is not entirely correct but partly reflects the limited energy window of the QENS study.

[44] D. Ostrovskii, L. M. Torell, G. B. Appetecchi, and B. Scrosati, Solid State Ionics **106**, 19 (1998).
[45] J.-C. Soetens, C. Millot, B. Maigret, and I. Bakó, J. Mol. Liq. **92**, 201 (2001).
[46] T. Nicolai and W. Brown, Macromolecules **29**, 1698 (1996).
[47] T. Uematsu, C. Svanberg, M. Nydén, and P. Jacobsson, Phys. Rev. E **68**, 051803 (2003).
[48] C. Svanberg, R. Bergman, P. Jacobsson, and L. Börjesson, Phys. Rev. B **66**, 054304 (2002).
[49] J. Spěváček and M. Suchopárek, Macromolecules **30**, 2178 (1997).
[50] A. Saiani, J. Spěváček, and J.-M. Guenet, Macromolecules **31**, 703 (1998).
[51] C. Svanberg, W. Pyckhout-Hintzen, and L. Börjesson (unpublished).
[52] D. J. Ward and G. R. Mitchell, Phys. Scr., T **T57**, 153 (1995).
[53] C. Svanberg, T. Uematsu, and P. Jacobsson (unpublished).